

Kinetic response of a photoperturbed allosteric protein

Brigitte Buchli^{a,1}, Steven A. Waldauer^{a,1}, Reto Walser^{a,1}, Mateusz L. Donten^a, Rolf Pfister^a, Nicolas Blöchliger^b, Sandra Steiner^b, Amedeo Caflisch^b, Oliver Zerbe^a, and Peter Hamm^{a,2}

Departments of ^aChemistry and ^bBiochemistry, University of Zurich, CH-8057 Zurich, Switzerland

Edited by Hans Frauenfelder, Los Alamos National Laboratory, Los Alamos, NM, and approved June 3, 2013 (received for review April 3, 2013)

By covalently linking an azobenzene photoswitch across the binding groove of a PDZ domain, a conformational transition, similar to the one occurring upon ligand binding to the unmodified domain, can be initiated on a picosecond timescale by a laser pulse. The protein structures have been characterized in the two photoswitch states through NMR spectroscopy and the transition between them through ultrafast IR spectroscopy and molecular dynamics simulations. The binding groove opens on a 100-ns timescale in a highly nonexponential manner, and the molecular dynamics simulations suggest that the process is governed by the rearrangement of the water network on the protein surface. We propose this rearrangement of the water network to be another possible mechanism of allostery.

Subtle conformational transitions within the folded state of highly structured proteins are often an integral aspect in their functional mechanism. These conformational transitions can occur as a result of different events, such as ligand binding, covalent modification (e.g., phosphorylation), or proteolytic cleavage. When an event or perturbation at one site in a protein changes the enzymatic activity or the binding affinity to a ligand at another distant site, this process can be described as allostery. Hemoglobin has long served as the prototypical example to study this effect, where the binding of an oxygen in one subunit modifies the affinity of binding oxygen in another subunit (1, 2). The traditional models of allostery developed by Monod et al. (3) and Koshland et al. (4) attribute allosteric effects to conformational changes by which the allosteric binding site communicates with the distant active site. There is, however, increasing evidence that allostery can be mediated also without any conformational change, relying purely on changes in internal protein dynamics (5).

PDZ domains are an important class of protein interaction modules that have been studied extensively in the context of allostery. They are found in a large variety of proteins and generally bind the C termini of their targets (6–11). As scaffolding domains, they are molecular switches that play a central role in signal transduction. For several PDZ domain proteins, allosteric interactions are an important regulatory mechanism (10, 12–15).

NMR spectroscopy has been particularly useful to elucidate the equilibrium dynamics of proteins on various timescales. The notion of allostery mediated through a change in dynamic properties was corroborated by a study of the third PDZ domain from the PSD-95/SAP90 protein (16). This protein contains an additional C-terminal α -helix (α_3), which shows no direct interaction with the peptide ligand. Removal of α_3 has a negligible effect on the structure of the PDZ core domain; however, it does lead to a large decrease in ligand binding affinity, which was shown to be entirely entropic in nature. Other studies have identified changes in (conformational) entropy of both backbone (17) and side-chain (18) dynamics in other systems to give rise to allosteric effects.

Here, we focus on the second PDZ (PDZ2) domain from human tyrosine-phosphatase 1E (hPTP1E), which has been demonstrated to possess allosteric properties (19). The PDZ domain is a small 96-residue protein with a binding groove between the α_2 -helix and the β_2 -strand (Fig. 1B). As mentioned

previously, side-chain dynamics in contiguous sectors spanning the whole protein have been the proposed allosteric mechanism (19–21), but in this case, ligand binding also results in a small but significant structural change, albeit being quite small (22–24) (Fig. 1B and Table 1). Furthermore, a number of computational and experimental studies have addressed signal transduction pathways in the PDZ2 model system (25–34).

Allostery is the propagation of a signal between two sites of a protein. Most of the investigations so far have addressed the question of what that signal might be, e.g., a structural change vs. a change in dynamic properties. Even less is known of how such a signal propagates. Whereas NMR spectroscopy is extremely powerful in elucidating equilibrium dynamics on many timescales through relaxation experiments, its inherent time resolution is rather limited in studies of nonequilibrium processes, such as signal propagation. Transient IR spectroscopy, in contrast, provides essentially unlimited (i.e., picosecond) direct time resolution together with still significant chemical selectivity.

To make the best use of the high time resolution, it is crucial to be able to perturb the system locally and with a short laser pulse. Ideally, one would phototrigger the association or dissociation of a ligand. Here, we take an experimentally more feasible approach by covalently linking an azobenzene derivative across the binding groove, which can be switched between *cis* and *trans* isomers with a light of different wavelengths (Fig. 1A) (35–38). We carefully designed the system such that the structural perturbation upon isomerization of the photoswitch mimics that upon ligand binding, as is discussed in the next section. Subsequently, we use transient IR spectroscopy to investigate the nonequilibrium transition between both states and finally use nonequilibrium molecular dynamics (MD) simulations to complement the experimental results with atomistic detail.

Structural Characterization

In close analogy to ref. 39, we identified the surface-exposed amino acid pair Ser21 and Glu76 as anchor points for the photoswitch because their C_α - C_α distances in the apo and holo forms closely match those of the photoswitch length in its two configurations. Furthermore, these two residues face across the binding groove at the center. The residues were mutated to cysteines to which the photoswitch was covalently coupled (Fig. S1) (40). When searching for the anchor points, we used the NMR ensemble of structures of the PDZ2 domain [holo, 1D5G, ref. 23]; apo, 3PDZ, ref. 22)], which reveals a rather large 1.5-Å change

Author contributions: A.C., O.Z., and P.H. designed research; B.B., S.A.W., R.W., M.L.D., N.B., S.S., and P.H. performed research; B.B., S.A.W., R.W., and R.P. contributed new reagents/analytic tools; B.B., S.A.W., R.W., O.Z., and P.H. analyzed data; and B.B., S.A.W., R.W., and P.H. wrote the paper.

The authors declare no conflict of interest.

This article is a PNAS Direct Submission.

Data deposition: The NMR, atomic coordinates, chemical shifts, and restraints have been deposited in the Protein Data Bank, www.pdb.org (PDB ID codes 2M0Z and 2M10) and the BioMagResBank, www.bmrb.wisc.edu (accession nos. 18833 and 18834).

¹B.B., S.A.W., and R.W. contributed equally to this work.

²To whom correspondence should be addressed. E-mail: phamm@pci.uzh.ch.

This article contains supporting information online at www.pnas.org/lookup/suppl/doi:10.1073/pnas.1306323110/-DCSupplemental.

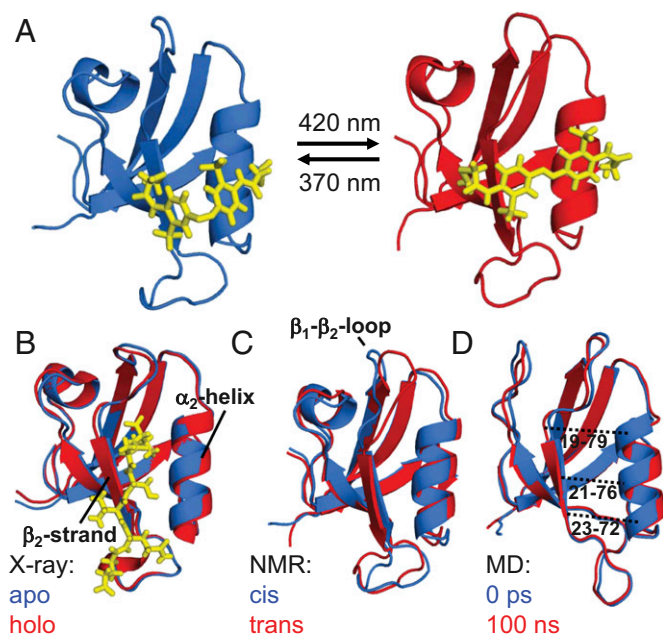


Fig. 1. (A) Averaged NMR structures of the photoswitchable PDZ2 domain with the photoswitch (yellow) in the *cis* (Left, PDB ID 2M0Z) and *trans* (Right, PDB ID 2M10) conformations. (B) Overlays of the apo (blue) and holo (red) X-ray structures [3LNK and 3LNY (24)] together with the ligand (the Ras guanine nucleotide exchange factor 2 C-terminal peptide, in yellow) in the latter case. (C) The NMR structures with the photoswitch in *cis* (blue) and in *trans* (red) and (D) the averaged MD structures with the photoswitch in *cis* (blue) and 100 ns after switching into *trans* (red). For clarity, the photoswitch is not shown in C and D. The dotted lines in D indicate the C_{α} - C_{α} distances shown in Fig. 4B.

(on average) for the $C_{\alpha}(21)$ - $C_{\alpha}(76)$ distance. Recently, X-ray crystallography (3LNK and 3LNY, ref. 24) has shown, however, that this change is about a factor of 2 smaller (i.e., 0.8 Å). The fact that the linker could nevertheless be successfully coupled and resulted in a stable, well-folded protein indicates that the possible structural perturbation is well tolerated.

The two equilibrium structures of the PDZ2 domain with the photoswitch in the *cis* and *trans* configurations were determined by NMR spectroscopy [see *SI Text* for details, Protein Data Bank (PDB) IDs 2M0Z and 2M10]. Whereas the *trans* form of the azobenzene photoswitch is predominant (~90%) after equilibration in the dark, the *cis* state was generated and maintained (>90%) by continuously illuminating the sample inside the spectrometer with a 370-nm laser coupled to a glass fiber leading into the NMR tube (for further information on the design see *SI Text*), similar to that described in previous work (41, 42). Both forms are stably folded and structurally similar to the corresponding X-ray structures (24), as can be seen in Fig. 1 B and C. More quantitatively, the rmsd of the NMR structure in *cis*

Table 1. Structural comparison

rmsd	X-ray (24): apo→holo	NMR: <i>cis</i> → <i>trans</i>	MD: <i>cis</i> → <i>trans</i>
All secondary	0.34	0.92	0.46
α_2 and β_2	0.41	0.80	0.62

Structural difference of the apo vs. the holo form deduced from the X-ray structures (3LNK and 3LNY, ref. 24) or the *cis* vs. the *trans* conformer from the NMR structures and the MD simulations, respectively. The first row reports the rmsd (in angstroms) when considering all backbone atoms of regions with defined secondary structure and the second row that when considering only the α_2 -helix and the β_2 -strand.

compared with the X-ray structure in the apo form is 1.0 Å and that of *trans* to the holo form is 1.1 Å (considering all backbone heavy atoms of only the regions with defined secondary structure). These values include the uncertainties in the structure determination, the different environments (crystal vs. solvent), and the fact that the molecule is modified by the photoswitch. Also the adaptation of the structure upon isomerization of the photoswitch is comparable to that upon ligand binding. Table 1 lists the rmsds between the corresponding structures for all secondary structure elements and for residues of the α_2 -helix and β_2 -strand only, with the latter constituting the binding groove. Our construct does slightly overemphasize the conformational perturbation, but the overall agreement is quite reasonable.

Transient IR Spectroscopy

Having established the equilibrium structures of the starting and final states by NMR spectroscopy, we now turn to IR spectroscopy. Fig. 2A displays stationary FTIR spectra in the region of the amide I band, which is a sensitive probe of the structure of the protein backbone. All IR experiments have been performed in a fully hydrated state [50 mM borate buffer (pH 8.5) and 150 mM NaCl, lyophilized and dissolved in D_2O at 1.3 mM concentration].

A difference signal upon switching *cis* → *trans* or *trans* → *cis* is clearly visible (Fig. 2A, red and green) with an intensity of about 1/50th that of the absolute amide I band (Fig. 2, blue), indicating that small changes in the protein backbone do indeed occur. The *trans* → *cis* difference spectrum, induced by illuminating a dark-adapted sample at 370 nm, and the *cis* → *trans* difference spectrum, after switching off the 370-nm light and subsequent relaxation back to *trans* in ~30 min, are mirror images of each other (Fig. 2A, green and red lines), confirming that the molecule can be switched reversibly. In the next step, to observe the

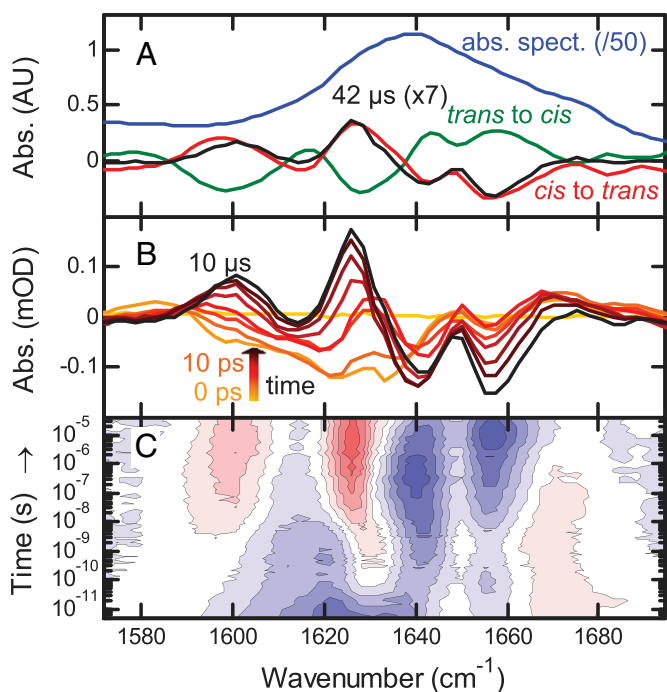


Fig. 2. (A) Absolute (photoswitch in *trans*, blue, downscaled by 50) and difference FTIR spectra (red and green) compared with the transient spectrum at 42 μ s (black, upscaled by 7). (B) Transient difference spectra at -1 ns (yellow), 0 ps (light orange), and from 10 ps to 10 μ s by decade (orange to black). (C) Contour plot of the IR response. Red indicates induced absorption, blue indicates a bleach, and contour lines are equally spaced.

transition in time-resolved experiments, we prepared all samples in the *cis* configuration by continuously illuminating them at 370 nm with an excess amount of light and then initiated the *cis* → *trans* transition with a picosecond 420-nm pulse (*Materials and Methods*). At long times (42 μs), the transient IR response in the amide I region closely resembles the shape of the steady state (Fig. 2A, black vs. red line), indicating that the structural transition is essentially complete after this time. Its amplitude is about one-seventh of the latter, allowing one to estimate the combined excitation probability and isomerization yield.

In reaching the final state, the data reveal a complex evolution over many orders of magnitude in time with bands that both change in intensity and shift in frequency (Fig. 2B and C). No physically meaningful model with a limited number of discrete intermediate states could be identified to which we could globally fit the data. Similar observations have been made for downhill folding (43, 44), with different kinetic responses for different spectroscopic observables. This behavior is indicative of a continuous transition between initial and final states without any significant barriers on the pathway.

Three major phases of the overall process can nonetheless be identified. We illustrate these phases in Fig. 3 for the amide I band, choosing 1,640 cm⁻¹ as probe wavelength (red circles), and a strong band at 1,491 cm⁻¹ originating from the photoswitch linked to the PDZ2 domain (Fig. 3, green circles). This band is the amide II vibration of the amide unit of the linker connecting the azobenzene moiety to the protein (Fig. S14). For comparison, the response of the same band of the unlinked photoswitch is shown as well (Fig. 3, blue circles; see Fig. S2, for the complete data). Phase I, clearly visible in the photoswitch bands in both the linked and unlinked form, is initiated by the absorption of a 420-nm photon and the subsequent ultrafast isomerization of the azobenzene moiety. This results in the deposition of a large amount of energy into the vibrational degrees of freedom of the molecule. The vibrational energy appears as heat and results in a broad IR signal, decaying within a few 10s of picoseconds as it quickly dissipates into the solvent (45). The heat signal happens to be zero for the amide I band at 1,640 cm⁻¹, but it is clearly visible at other probe wavelengths (Fig. 2C).

Subsequently, in phase II, the band of the photoswitch linked to the PDZ2 domain evolves in a highly nonexponential manner until about 100 ns (Fig. 3, green circles), significantly slower than that of the photoswitch alone (Fig. 3, blue circles).

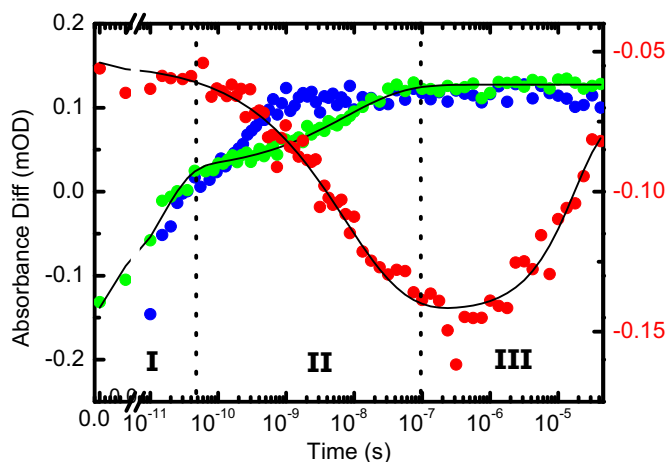


Fig. 3. Amide I response at a selected wavelength of 1,640 cm⁻¹ (red, right scale) compared with that of a band at 1,491 cm⁻¹ from the unlinked photoswitch (blue, left scale) and with that of the same band of the photoswitch linked to the PDZ2 domain (green, left scale). The signal of the photoswitchable PDZ2 domain (red and green) is fitted jointly to Eq. 1 (black).

Photoisomerization of the azobenzene moiety is an ultrafast picosecond process (46). The heat signal of the photoswitch linked to the protein appears on the same timescale as that of the unlinked photoswitch (Fig. S2); hence, in terms of crossing from the electronically excited back to the ground state, and thus in terms of the configuration of the central N = N bond, isomerization is equally fast in both cases. When bound to the protein, however, the photoswitch will find itself in a highly strained state after isomerization, because the protein cannot adapt instantaneously. This strain will affect also the vibrational states of the linker connecting the azobenzene moiety to the protein, i.e., the 1,491-cm⁻¹ band. As the protein relaxes, the strain on the photoswitch is slowly released. Hence, the phase II signal of the photoswitch (Fig. 3, green circles) can be thought of as an indirect measure of the perturbation of the binding groove, as the binding groove is cross-linked by the photoswitch. Similar conclusions have been drawn for the electronic response of a similar azo-photoswitch in a smaller peptide (36). The perturbation of the binding groove is also reflected in the amide I band of the protein (Fig. 3, red circles).

Finally, in phase III, the photoswitch signal remains constant, because the binding groove has fully adapted to the perturbation. The amide I signal nevertheless continues to evolve in time. We assume that this signal is related to a slight rearrangement of the protein structure in a region different from the binding groove, for instance of some of the turn regions that are known to be quite flexible. This interpretation is corroborated by signal broadening of NMR resonances from the β₁-β₂ loop.

The two time traces from the photoswitchable PDZ2 domain at 1,640 cm⁻¹ and at 1,491 cm⁻¹ can be fitted jointly to a function (Fig. 3, black lines)

$$q(t) = a_0 + a_1 e^{-(t/\tau_1)} + a_2 e^{-(t/\tau_2)^\beta} + a_3 e^{-(t/\tau_3)}, \quad [1]$$

which is composed of a fast exponential contribution for the heat signal decay in phase I (τ₁ = 15 ps), a stretched exponential contribution for the binding groove perturbation in phase II (τ₂ = 7 ns, β = 0.49), and another exponential contribution (τ₃ = 20 μs) for the final relaxation in the amide I band in phase III. In that fit, the time constants and the stretching factor were forced to be the same for both time traces, but the amplitudes were allowed to differ (Table S1). With a stretching factor of β = 0.49, the nonexponential time dependence of phase II is quite pronounced.

Nonequilibrium Molecular Dynamics

To facilitate the understanding of the transition on an atomistic level, we used nonequilibrium MD simulations in explicit water. Starting from an equilibrated *cis* ensemble (with an rmsd to the corresponding NMR structure of 1.4 Å), we launched very many nonequilibrium trajectories by instantaneously switching the potential energy function of the central N = N bond of the photoswitch from one that is stable in *cis* to one that is stable in *trans* (*Materials and Methods*) (36, 38, 47). As these simulations are limited to a maximum simulation time of 100 ns, we focus on phase II in the following discussion, i.e., the perturbation of the binding groove. The overall fold does not change during the first 100 ns after photoswitching (Fig. 1D), but the protein backbone is deformed slightly, as expressed by the rmsd that increases to 0.46 Å after 100 ns (Table 1 and Fig. 4A). The rmsd is larger when considering the α₂-helix and the β₂-strand only (0.62 Å), emphasizing that most of the structural changes occur at the binding groove on this timescale. As a function of time, the rmsd jumps relatively rapidly within the first 1 ps. It then continues to grow in a highly nonexponential manner, covering all orders of magnitude in time considered in this simulation, similar to the experimental observation (Fig. 3, green circles), and in fact it is

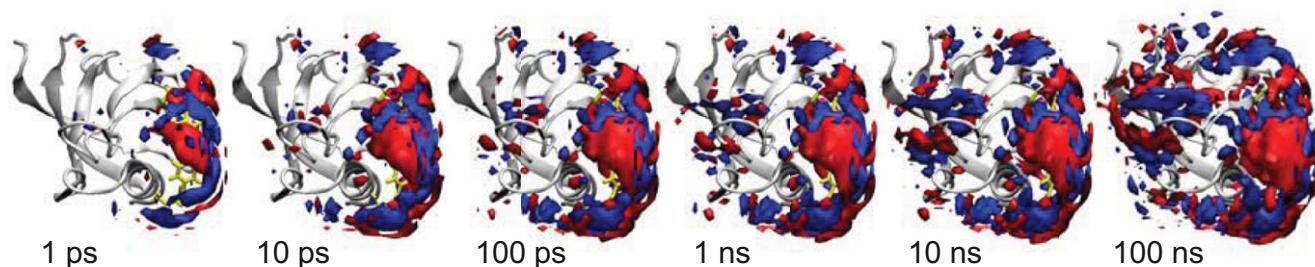


Fig. 5. Change of water density as a function of simulation time, compared with that just before switching. Red depicts increased density and blue decreased density. The contour surfaces correspond to changes of ± 0.01 water/ \AA^3 (for comparison, the bulk water density is ~ 0.033 water/ \AA^3). The protein is shown as a gray ribbon and the photoswitch (visible only in part) is shown in yellow. See also [Movie S1](#).

and the native state of a four-helix bundle protein (58). We find that in our system the overall protein response is dominated by the rearrangement of the water network on the protein surface. Interestingly, the perturbation of the water network propagates around the protein within the 100 ns (Fig. 5).

We propose this to be another possible mechanism of allostery, which addresses the question of how the ligand binding site communicates with remote parts of the protein. Although the photoswitch is a rather crude mimic of ligand binding, the peptide ligand will still introduce new partial charges in the binding pocket that will rearrange the water network in its vicinity and eventually also at larger distances. This mechanism would work without any significant structural change of the protein and might even unify the seemingly competing points of view, which explain allostery either as a structural or as a dynamical effect. That is, to the extent that the dynamics of a protein are slaved by water, a change in water structure can affect the dynamics of the protein. Independent from that, phase III in Fig. 3 also hints toward a conformational change of the protein backbone in a region different from the binding groove that also could be responsible for allosteric signaling in a more traditional sense (3, 4).

Materials and Methods

Protein Preparation. The PDZ2 domain (S21C E76C) was expressed from *Escherichia coli*, using standard methods. The photoswitch 3,3'-bis(sulfonato)-4,4'-bis(chloroacetamido)azobenzene (BSBCA) was covalently linked to the two cysteines (40); see [SI Text](#) and [Fig. S3](#) for details. We learned from mass spectrometry that the protein reacts photochemically with oxygen as well as with the initially used Tris buffer under the influence of the 420-nm laser pulses in the pump-probe experiment, where both presumably bind to the thioether groups of the cysteines linked to the photoswitch ([Fig. S4](#)). The experiments were therefore performed in 50 mM borate buffer (pH 8.5) and 150 mM NaCl, lyophilized and dissolved in D_2O , and care was taken to maintain the sample oxygen-free.

Time-Resolved IR Spectroscopy. Two synchronized 1-kHz Ti:sapphire oscillator/regenerative amplifier femtosecond laser systems (Spectra Physics) were used for pump-probe measurements (59). The jitter between both lasers (which effectively determines the time resolution of the experiment) was ~ 10 ps

and the delay could be adjusted up to 42 μ s. The frequency-doubled pulses (420 nm, 3 μ J per pulse focused onto an ~ 200 - μ m beam diameter in the sample and stretched to ~ 1 ps to reduce sample deposition on the cuvette windows) of one laser system were used to excite the photoswitch. The IR probe pulses were obtained by sending the output of the second laser system through an optical parametric amplifier (100 fs, center wavenumber 1,635 cm^{-1} or 1,443 cm^{-1}). The sample was circulated in a closed-cycle flow-cell system consisting of a reservoir followed by a CaF_2 sample cell with 50 μ m optical path length. The reservoir was continuously illuminated with a 150-mW, 370-nm continuous wave diode laser (CrystaLaser) so that all protein flowing into the sample cell was in the *cis* configuration.

NMR. NMR spectra of PDZ2 with the photoswitch in *trans* were recorded in the dark after equilibration. For all measurements with the photoswitch in the *cis* configuration, the sample was continuously illuminated with the 370-nm cw laser specified above ([Fig. S5](#)) coupled into the NMR spectrometer through a custom-fabricated fiber terminated with an extended cylindrical diffuser (Molex). Spectrum assignment was achieved with a standard set of triple-resonance experiments. Structure calculation was performed from NOE distance restraints from ^{15}N - and ^{13}C -resolved NOESY spectra with 75-ms mixing times. NOE data were complemented by amide proton residual dipolar couplings (NH-RDCs) measured in Pf1 bacteriophage and *n*-dodecyl-penta(ethylene glycol)/*n*-hexanol liquid crystalline medium. The 20 conformers with lowest energy of both structures showed no NOE violations bigger than 0.5 \AA and showed good Ramachandran plot statistics with only 0.3% of the residues in disallowed regions (for more detailed description of experiments, parameters, and structural statistics see [SI Text](#) and [Tables S2](#) and [S3](#)).

Computational Methods. MD simulations were performed with the Gromacs program package (60) and the Gromacs implementation of the Charmm27 force field (61, 62). The photoswitch was parameterized as in ref. 36. Details of the simulation protocol are given in [SI Text](#).

ACKNOWLEDGMENTS. We thank Ben Schuler and his group, in particular Hagen Hofmann, for tremendous help with the protein chemistry; and Andrew Woolley and Gerhard Stock for important discussions; and the Functional Genomics Center Zurich, especially Serge Chesnov, for help with mass spectrometry. This work has primarily been supported by an European Research Council (ERC) Advanced Investigator Grant (DYNALLO) and in part by the Swiss National Science Foundation through the National Center of Competence and Research (NCCR) MUST.

- Henry ER, Jones CM, Hofrichter J, Eaton WA (1997) Can a two-state MWC allosteric model explain hemoglobin kinetics? *Biochemistry* 36(21):6511–6528.
- Eaton WA, Henry ER, Hofrichter J, Mozzarelli A (1999) Is cooperative oxygen binding by hemoglobin really understood? *Nat Struct Biol* 6(4):351–358.
- Monod J, Wyman J, Changeux JP (1965) On the nature of allosteric transitions - a plausible model. *J Mol Biol* 12:88–118.
- Koshland DE, Jr., Némethy G, Filmer D (1966) Comparison of experimental binding data and theoretical models in proteins containing subunits. *Biochemistry* 5(1): 365–385.
- Cooper A, Dryden DTF (1984) Allostery without conformational change. A plausible model. *Eur Biophys J* 11(2):103–109.
- Songyang Z, et al. (1997) Recognition of unique carboxyl-terminal motifs by distinct PDZ domains. *Science* 275(5296):73–77.
- Daniels DL, Cohen AR, Anderson JM, Brünger AT (1998) Crystal structure of the hCASK PDZ domain reveals the structural basis of class II PDZ domain target recognition. *Nat Struct Biol* 5(4):317–325.
- Harris BZ, Lim WA (2001) Mechanism and role of PDZ domains in signaling complex assembly. *J Cell Sci* 114(Pt 18):3219–3231.
- Jemth P, Gianni S (2007) PDZ domains: Folding and binding. *Biochemistry* 46(30): 8701–8708.
- Lee H-J, Zheng JJ (2010) PDZ domains and their binding partners: Structure, specificity, and modification. *Cell Commun Signal* 8:8.
- van Ham M, Hendriks W (2003) PDZ domains-glue and guide. *Mol Biol Rep* 30(2):69–82.
- van den Berk LCJ, et al. (2007) An allosteric intramolecular PDZ-PDZ interaction modulates PTP-BL PDZ2 binding specificity. *Biochemistry* 46(47):13629–13637.
- Li J, Callaway DJE, Bu Z (2009) Ezrin induces long-range interdomain allostery in the scaffolding protein NHERF1. *J Mol Biol* 392(1):166–180.
- Wilken C, Kitzing K, Kurzbauer R, Ehrmann M, Clausen T (2004) Crystal structure of the DegS stress sensor: How a PDZ domain recognizes misfolded protein and activates a protease. *Cell* 117(4):483–494.
- Whitney DS, Peterson FC, Volkman BF (2011) A conformational switch in the CRIB-PDZ module of Par-6. *Structure* 19(11):1711–1722.

16. Petit CM, Zhang J, Sapienza PJ, Fuentes EJ, Lee AL (2009) Hidden dynamic allostery in a PDZ domain. *Proc Natl Acad Sci USA* 106(43):18249–18254.
17. Popovych N, Sun S, Ebright RH, Kalodimos CG (2006) Dynamically driven protein allostery. *Nat Struct Mol Biol* 13(9):831–838.
18. Frederick KK, Marlow MS, Valentine KG, Wand AJ (2007) Conformational entropy in molecular recognition by proteins. *Nature* 448(7151):325–329.
19. Fuentes EJ, Der CJ, Lee AL (2004) Ligand-dependent dynamics and intramolecular signaling in a PDZ domain. *J Mol Biol* 335(4):1105–1115.
20. Fuentes EJ, Gilmore SA, Mauldin RV, Lee AL (2006) Evaluation of energetic and dynamic coupling networks in a PDZ domain protein. *J Mol Biol* 364(3):337–351.
21. Gianni S, et al. (2006) Demonstration of long-range interactions in a PDZ domain by NMR, kinetics, and protein engineering. *Structure* 14(12):1801–1809.
22. Kozlov G, Gehring K, Ekiel I (2000) Solution structure of the PDZ2 domain from human phosphatase hPTP1E and its interactions with C-terminal peptides from the Fas receptor. *Biochemistry* 39(10):2572–2580.
23. Kozlov G, Banville D, Gehring K, Ekiel I (2002) Solution structure of the PDZ2 domain from cytosolic human phosphatase hPTP1E complexed with a peptide reveals contribution of the beta2-beta3 loop to PDZ domain-ligand interactions. *J Mol Biol* 320(4):813–820.
24. Zhang J, et al. (2010) Crystallographic and nuclear magnetic resonance evaluation of the impact of peptide binding to the second PDZ domain of protein tyrosine phosphatase 1E. *Biochemistry* 49(43):9280–9291.
25. Ota N, Agard DA (2005) Intramolecular signaling pathways revealed by modeling anisotropic thermal diffusion. *J Mol Biol* 351(2):345–354.
26. De Los Rios P, et al. (2005) Functional dynamics of PDZ binding domains: A normal-mode analysis. *Biophys J* 89(1):14–21.
27. Sharp K, Skinner JJ (2006) Pump-probe molecular dynamics as a tool for studying protein motion and long range coupling. *Proteins* 65(2):347–361.
28. Dhulesia A, Gsponer J, Vendruscolo M (2008) Mapping of two networks of residues that exhibit structural and dynamical changes upon binding in a PDZ domain protein. *J Am Chem Soc* 130(28):8931–8939.
29. Kong Y, Karplus M (2009) Signaling pathways of PDZ2 domain: A molecular dynamics interaction correlation analysis. *Proteins* 74(1):145–154.
30. Gerek ZN, Ozkan SB (2011) Change in allosteric network affects binding affinities of PDZ domains: Analysis through perturbation response scanning. *PLoS Comput Biol* 7(10):e1002154.
31. Cilia E, Vuister GW, Lenaerts T (2012) Accurate prediction of the dynamical changes within the second PDZ domain of PTP1E. *PLoS Comput Biol* 8(11):e1002794.
32. Lockless SW, Ranganathan R (1999) Evolutionarily conserved pathways of energetic connectivity in protein families. *Science* 286(5438):295–299.
33. Süel GM, Lockless SW, Wall MA, Ranganathan R (2003) Evolutionarily conserved networks of residues mediate allosteric communication in proteins. *Nat Struct Biol* 10(1):59–69.
34. Chi CN, et al. (2008) Reassessing a sparse energetic network within a single protein domain. *Proc Natl Acad Sci USA* 105(12):4679–4684.
35. Kumita JR, Smart OS, Woolley GA (2000) Photo-control of helix content in a short peptide. *Proc Natl Acad Sci USA* 97(8):3803–3808.
36. Spörlein S, et al. (2002) Ultrafast spectroscopy reveals subnanosecond peptide conformational dynamics and validates molecular dynamics simulation. *Proc Natl Acad Sci USA* 99(12):7998–8002.
37. Rehm S, Lenz MO, Mensch S, Schwalbe H, Wachtveitl J (2005) Ultrafast spectroscopy of a photoswitchable 30-amino acid de novo synthesized peptide. *Chem Phys* 323(1):28–35.
38. Ihalainen JA, et al. (2008) α -Helix folding in the presence of structural constraints. *Proc Natl Acad Sci USA* 105(28):9588–9593.
39. Zhang F, et al. (2009) Structure-based approach to the photocontrol of protein folding. *J Am Chem Soc* 131(6):2283–2289.
40. Burns DC, Zhang F, Woolley GA (2007) Synthesis of 3,3'-bis(sulfonato)-4,4'-bis(chloroacetamido)azobenzene and cysteine cross-linking for photo-control of protein conformation and activity. *Nat Protoc* 2(2):251–258.
41. Rubinstenn G, et al. (1998) Structural and dynamic changes of photoactive yellow protein during its photocycle in solution. *Nat Struct Biol* 5(7):568–570.
42. Kühn T, Schwalbe H (2000) Monitoring the kinetics of ion-dependent protein folding by time-resolved nmr spectroscopy at atomic resolution. *J Am Chem Soc* 122:6169–6174.
43. Garcia-Mira MM, Sadqi M, Fischer N, Sanchez-Ruiz JM, Muñoz V (2002) Experimental identification of downhill protein folding. *Science* 298(5601):2191–2195.
44. Ma H, Gruebele M (2005) Kinetics are probe-dependent during downhill folding of an engineered lambda6-85 protein. *Proc Natl Acad Sci USA* 102(7):2283–2287.
45. Hamm P, Ohline SM, Zinth W (1997) Vibrational cooling after ultrafast photoisomerization of azobenzene measured by femtosecond infrared spectroscopy. *J Chem Phys* 106:519–529.
46. Nägele T, Hoche R, Zinth W, Wachtveitl J (1997) Femtosecond photoisomerization of cis-azobenzene. *Chem Phys Lett* 272:489–495.
47. Nguyen PH, Stock G (2006) Nonequilibrium molecular dynamics simulation of a photoswitchable peptide. *Chem Phys* 323:36–44.
48. Mahoney MW, Jorgensen WL (2001) Diffusion constant of the tip5p model of liquid water. *J Chem Phys* 114:363–366.
49. Lim M, Jackson TA, Anfinsen PA (1993) Nonexponential protein relaxation: Dynamics of conformational change in myoglobin. *Proc Natl Acad Sci USA* 90(12):5801–5804.
50. Frauenfelder H, Sligar SG, Wolynes PG (1991) The energy landscapes and motions of proteins. *Science* 254(5038):1598–1603.
51. Frauenfelder H, et al. (2009) A unified model of protein dynamics. *Proc Natl Acad Sci USA* 106(13):5129–5134.
52. Volk M, et al. (1997) Peptide conformational dynamics and vibrational Stark effects following photoinitiated disulfide cleavage. *J Phys Chem B* 101:8607–8616.
53. Yang H, et al. (2003) Protein conformational dynamics probed by single-molecule electron transfer. *Science* 302(5643):262–266.
54. Milanese L, et al. (2012) Measurement of energy landscape roughness of folded and unfolded proteins. *Proc Natl Acad Sci USA* 109(48):19563–19568.
55. Jäcke J (1986) Models of the glass transition. *Rep Prog Phys* 49:171–231.
56. Fenimore PW, Frauenfelder H, McMahon BH, Parak FG (2002) Slaving: Solvent fluctuations dominate protein dynamics and functions. *Proc Natl Acad Sci USA* 99(25):16047–16051.
57. Vitkup D, Ringe D, Petsko GA, Karplus M (2000) Solvent mobility and the protein 'glass' transition. *Nat Struct Biol* 7(1):34–38.
58. Sekhar A, Vallurupalli P, Kay LE (2012) Folding of the four-helix bundle FF domain from a compact on-pathway intermediate state is governed predominantly by water motion. *Proc Natl Acad Sci USA* 109(47):19268–19273.
59. Bredenbeck J, Helbing J, Hamm P (2004) Continuous scanning from picoseconds to microseconds in time resolved linear and nonlinear spectroscopy. *Rev Sci Instrum* 75(11):4462.
60. Van Der Spoel D, et al. (2005) GROMACS: Fast, flexible, and free. *J Comput Chem* 26(16):1701–1718.
61. Mackerell AD, Jr., Feig M, Brooks CL, 3rd (2004) Extending the treatment of backbone energetics in protein force fields: Limitations of gas-phase quantum mechanics in reproducing protein conformational distributions in molecular dynamics simulations. *J Comput Chem* 25(11):1400–1415.
62. Mackerell AD, et al. (1998) All-atom empirical potential for molecular modeling and dynamics studies of proteins. *J Phys Chem B* 102:3586–3616.